Nuclear Engineering and Technology 49 (2017) 1740–1747

Contents lists available at ScienceDirect

Nuclear Engineering and Technology

journal homepage: www.elsevier.com/locate/net

Original Article

Allowable peak heat-up cladding temperature for spent fuel integrity during interim-dry storage

Ki-Nam Jang, Hyun-Jin Cha, Kyu-Tae Kim*

Dongguk University, College of Energy and Environment, 123 Dongdae-ro, Gyeongju, Gyeongbuk 38066, Republic of Korea

ARTICLE INFO

Article history:
Received 4 February 2017
Received in revised form
30 June 2017
Accepted 9 August 2017
Available online 1 September 2017

Keywords:
Hydride-induced fracture
Hydride reorientation
Terminal cool-down temperature
Zirconium alloy

ABSTRACT

To investigate allowable peak cladding temperature and hoop stress for maintenance of cladding integrity during interim-dry storage and subsequent transport, zirconium alloy cladding tubes were hydrogen-charged to generate 250 ppm and 500 ppm hydrogen contents, simulating spent nuclear fuel degradation. The hydrogen-charged specimens were heated to four peak temperatures of 250°C, 300°C, 350°C, and 400°C, and then cooled to room temperature at cooling rates of 0.3 °C/min under three tensile hoop stresses of 80 MPa, 100 MPa, and 120 MPa. The cool-down specimens showed that high peak heat-up temperature led to lower hydrogen content and that larger tensile hoop stress generated larger radial hydride fraction and consequently lower plastic elongation. Based on these out-of-pile cladding tube test results only, it may be said that peak cladding temperature should be limited to a level < 250°C, regardless of the cladding hoop stress, to ensure cladding integrity during interim-dry storage and subsequent transport.

1. Introduction

The life cycle of pressurized water reactor (PWR) fuel is divided into fresh fuel fabrication, fuel irradiation in a reactor, wet storage of spent fuel in a spent fuel pit, vacuum drying of spent fuel, dry storage of spent fuel in an interim facility, and subsequent spent fuel transport for reuse or final disposal. From Fig. 1, it can be seen that the cladding temperature may vary depending on the vacuum drying environment. Considering that hydride reorientation of spent fuel during interim-dry storage strongly depends on the peak cladding temperature and tensile hoop stress [1,2], it may be said that differences in peak cladding temperature generated by various vacuum drying processes will result in different amounts of radial hydrides during interim-dry storage.

It was reported that there are three cladding tube failure modes during transportation accidents involving spent fuel, including transport tearing (Mode I), rod breakage (Mode II), and longitudinal tearing (Mode III) [3]. It was also reported that failure Mode-I is initiated under bending type deformations, and can potentially expand to failure Mode-II. Neither of these modes engage radial hydrides, in contrast to failure Mode-III which, because of the effect of radial hydrides, is likely to dominate the evolution of cladding failure during transportation accidents. It was reported that the radial hydride fraction in the cladding tube occurring during interim-dry storage can vary due to different peak cladding temperatures generated by various vacuum drying processes, burn-up dependent hydrogen contents and oxide thicknesses, tensile hoop stresses, and cooling rates during interim-dry storage [4]. Therefore, minimization of radial hydride precipitation in the cladding tube is a key factor for spent fuel integrity during interim-dry storage and transportation accidents.

Minimizing radial hydride precipitation through operational restrictions is the primary objective of Interim Staff Guidance–11 (ISG-11), revision 3 [5], which limits the peak cladding temperature to 400°C, with corresponding limitation on the number of thermal cycles during cask loading, drying and helium gas charging. It is generally known that the hydrogen content in the PWR cladding tube and the fuel rod internal pressure should be < 600 ppm-H and the reactor coolant system pressure should be < 15.5 MPa. The rod internal pressure of 15.5 MPa may cause a tensile hoop stress of 150 MPa on the cladding tube when the cladding external pressure drops to atmospheric pressure. The tensile hoop stress of 150 MPa on the cladding tube may drop to < 120 MPa due to the considerable temperature decrease in the spent fuel during wet and dry storage. It was reported that the cladding tube may cool over several decades by ~100°C every 10 years (2×10^{-5} °C/min) during

* Corresponding author.
E-mail address: ktkim@dongguk.ac.kr (K.-T. Kim).

http://dx.doi.org/10.1016/j.net.2017.08.012

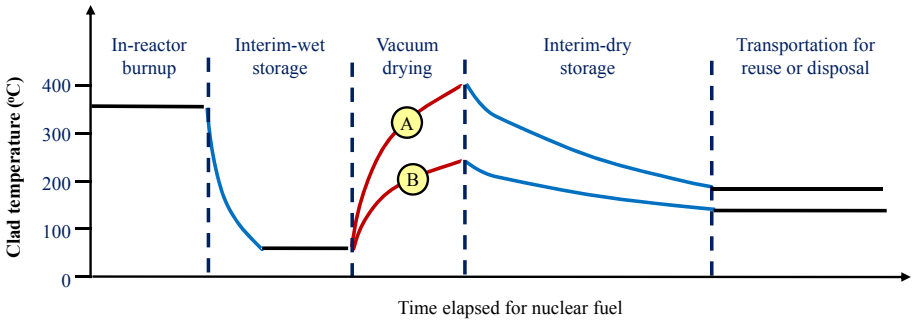

Fig. 1. Cladding temperature variation during nuclear fuel life cycle.

interim-dry storage [6]. It should be noted that Zr–Nb alloy cladding tubes have mostly been used for PWRs in the U.S.A and Korea.

To investigate the effects of hydrogen content in the cladding, peak cladding temperature and cladding hoop stress on the radial hydride precipitation during the spent fuel cool-down process in this study, the Zr–Nb alloy cladding tubes were charged with hydrogen gas, reaching levels of 250 ppm-H and 500 ppm-H; they were then machined into several ring specimens. The ring specimens were heated to the four prospective peak cladding temperatures of 250°C, 300°C, 350°C, and 400°C, and were then cooled at a cooling rate of 0.3 °C/min (furnace cooling) under three tensile hoop stresses of 80 MPa, 100 MPa, and 120 MPa. The behavior of the radial hydride precipitate obtained in this study may be used to evaluate the adequacy of the peak cladding temperature of 400°C, required by the ISG-11 [5], and to propose limiting operation conditions for the vacuum dying process and interim-dry storage.

It should be noted that the aforementioned test conditions employed in this work may not exactly simulate the behaviors of spent fuel claddings in interim dry storage, considering irradiation-induced damage, cladding oxide layer thicknesses, hydrogen content variations in the cladding, various cooling rates in interim dry storage, etc., in the PWR spent fuel. Any application of data for unirradiated specimens obtained in this work to predict cladding hydride reorientation behaviors and relevant mechanical property degradation in interim dry storage is far from being straightforward. Therefore, the results obtained in this study may be used qualitatively and restrictively to predict the amount of precipitated radial hydrides, the radial hydride-induced mechanical property degradation and the allowable cladding peak temperatures for spent fuel claddings in interim dry storage.

2. Materials and methods

Table 1 summarizes the chemical compositions including oxygen content, texture, and dimensions of the stress-relieved Zr–Nb alloy cladding tubes used in this study; all materials were supplied by the Korea Nuclear Fuel Company at Daejeon in Korea. Prior to hydrogen charging, the Zr–Nb cladding tubes were cut into several parts having lengths of 100 mm each; then, the tube surfaces were cleaned with acetic acid. To generate a uniform distribution of hydrogen through the tubes, two parts of the tubes were charged with hydrogen in a vacuum furnace at 400°C containing a mixture gas of hydrogen (150 torr) and helium (200 torr) [7]. The hydrogen concentrations of the test specimens were analyzed by the LECO hydrogen analyzer RH600 provided by the LECO corp. at Saint Joseph in MIchigan in the U.S.A. These hydrogen-charged specimens were found to contain respective hydrogen concentrations of 250 ± 25 ppm and 500 ± 25 ppm.

Table 1
Zirconium alloy cladding tubes used in this work.

Materials	Chemical composition (w/o)	Texture (Kearns no.)	Tube dimension (mm)
Zr alloy	Zr-1.0Nb-1.0 Sn-0.1Fe-0.12O	f_r (radial) = 0.62 f_t (tangential) = 0.26 f_a (axial) = 0.12	Outer dia = 9.50 Thickness = 0.57

dia, diameter; w/o, weight percent.

Fig. 2 shows a schematic configuration of the ring specimen and the two half-cylinder loading pins that open and strain the ring specimen. The ring specimens were cut transversely from the cladding tubes to make a width of 5 mm. The diameter of the half-cylinder loading pin was 8.35 mm and the gauge length of the specimens was 2.5 mm. Special grips were designed and fabricated to fix the loading pins and apply some tensile load to the specimen. Fig. 3 shows a calculated tensile hoop stress curve obtained by the thick wall assumption when applying an average stress of 80 MPa to the cladding. From this figure, it can be seen that tensile hoop stress decreases when moving from the cladding inner surface to the cladding outer surface. As can be seen in Fig. 4, the specimens were heated at 3.0 °C/min to the four peak cladding temperatures of 250°C, 300°C, 350°C, and 400°C and remained for 2 h at those peak cladding temperatures. Each specimen at its peak temperature, under no stress state, was quenched to room temperature to freeze the hydride distribution at the peak temperatures. However, the specimens were cooled from the four peak cladding temperatures in a furnace at a cooling rate of 0.3 °C/min under three tensile hoop stresses of 80 MPa, 100 MPa, and 120 MPa. Heat-up and cool-down tests were carried out using the KLES 500-Screep tester provided by the KLES inc. at Daejeon in Korea. To check the reproducibility of the test results, the cooling tests were repeated twice using the same batch of the specimens. Before and after the heat-up and cool-down tests, the specimens were cut in the middle of the gauge section along a line parallel to the axial direction of the cladding tube; the cut sections were examined by optical microscopy to reveal the fractions of radial and circumferential hydrides and their lengths. The etchant used for metallographic examination was composed of HF, HNO_3, and H_2O at a volume ratio of 10:45:45.

3. Results and discussion

Comparison of the optical micrographs obtained from the quenched specimens from 400°C to room temperature (RT) under no stress state indicates that most of the hydrides in the 250 ppm-H specimens were dissolved at the heat-up peak temperature of 400°C, whereas about half of the hydrides in the 500 ppm-H specimens were dissolved at that temperature. This hydride dissolution behavior may be explained by the terminal solid solubility for dissolution [8]. In Fig. 5, it can be seen that the hydrogen

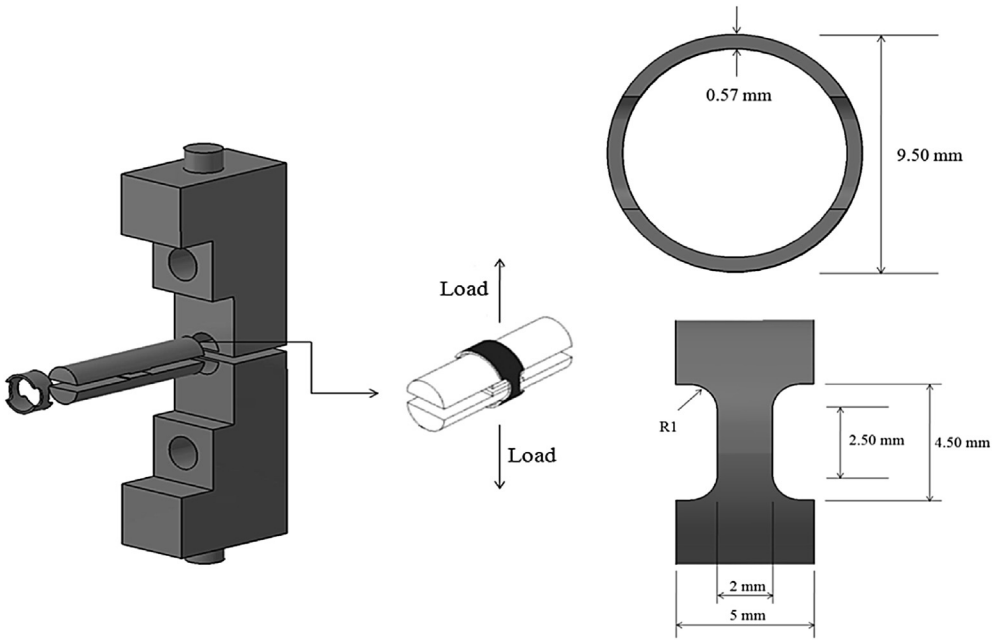

Fig. 2. Jigs and cladding tube specimen configurations.

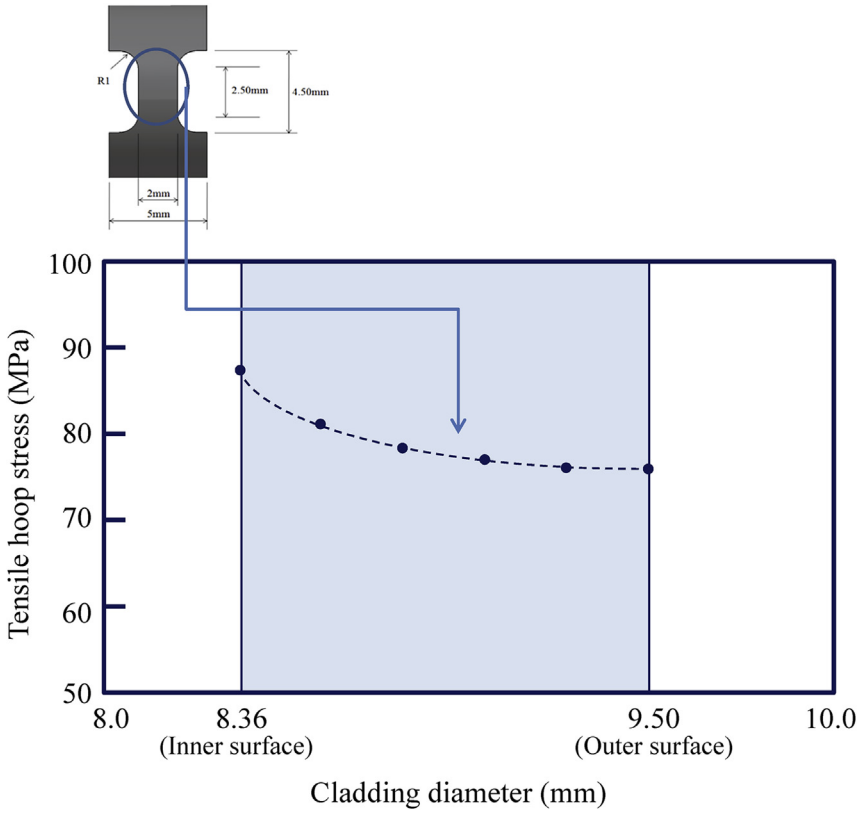

Fig. 3. Tensile hoop stress variation through the cladding thickness at the gauge section.

solubility for dissolution at the peak temperatures of 250°C, 300°C, 350°C, and 400°C are 45 ppm, 80 ppm, 150 ppm, and 230 ppm, respectively, indicating that most of the hydrides in the 250 ppm-H specimens may be dissolved at the heat-up peak temperature of 400°C, whereas about half of the hydrides in the 500 ppm-H may be dissolved at that temperature.

The heat-up specimens at the respective peak temperatures were cooled in the furnace to room temperature at a cooling rate of 0.3 °C/min under three tensile hoop stresses of 80 MPa, 100 MPa, and 120 MPa, as shown in Fig. 4. The optical micrographs obtained from the cool-down specimens for the four peak temperatures to RT under hoop stress state are shown in Fig. 6. In general, it is found

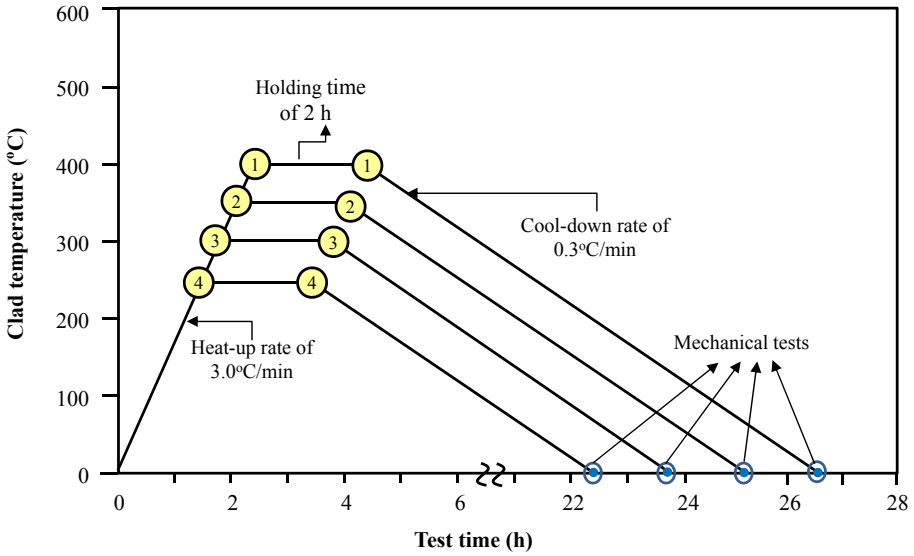

Fig. 4. Simulation of vacuum drying and interim-dry cooling periods for used nuclear fuel.

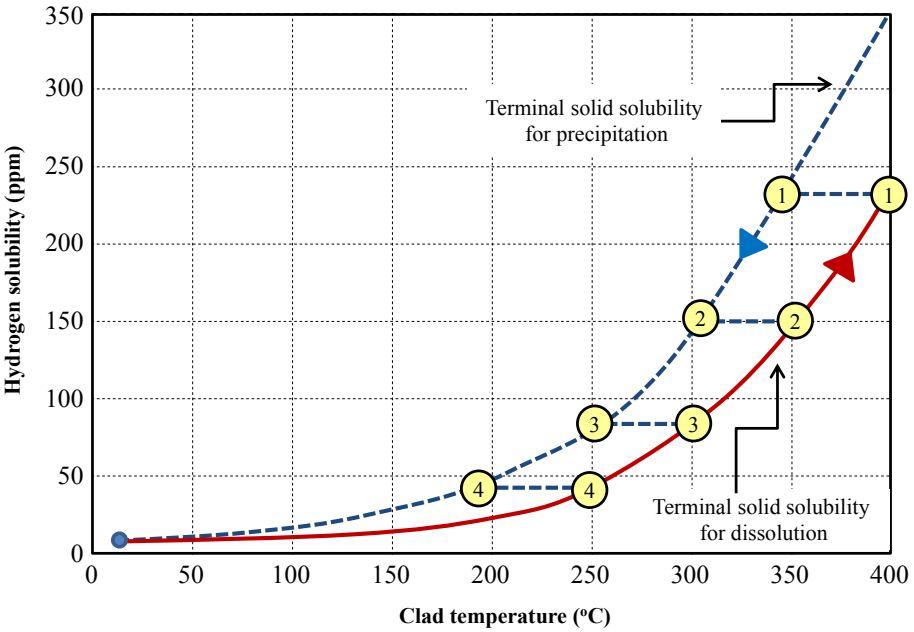

Fig. 5. Terminal solid solubility of hydrogen in zirconium alloy claddings.

that the radial hydride fraction in the inner region is larger than that in the outer region. This phenomenon may be explained by the difference in the cladding tensile hoop stress, which decreases from the inner region to the outer region, as explained in the experimental section, resulting in radial hydrides being more easily precipitated in the inner region under cooling to room temperature. Therefore, to maintain conservatism of the limiting tensile hoop stress, using the 500 magnified optical micrographs, the radial hydride fractions and average lengths were determined with an image analysis program that considered only the inner regions of the specimens, which generated relatively larger radial hydrides.

In order to calculate the radial hydride fraction from the optical micrographs shown in Fig. 6, the circumferential and radial hydrides were defined as follows. A circumferential hydride is defined as having plates with orientation within 0–40° of the circumferential axis, whereas a radial hydride was one that had orientation within 50–90° of the circumferential axis. The small fraction of hydrides within 40–50° of the circumferential axis was not counted as part of the radial or circumferential hydrides. The radial hydride fraction is defined as the ratio of the number of radial hydrides to the number of total hydrides.

Based on the procedures described above, the radial hydride fractions for the 250 ppm-H and 500 ppm-H specimens are given in Figs. 7 and 8, respectively. It is noteworthy that the uncertainty in the radial hydride fraction is < 5% of the average values. This uncertainty was estimated from the radial hydride fractions of the six portions within the box given in the optical micrographs shown in Fig. 6. From the data shown in Figs. 7 and 8, outstanding phenomena may be pointed out as follows. When cooled from the peak heat-up temperatures to room temperature, the 250 ppm-H

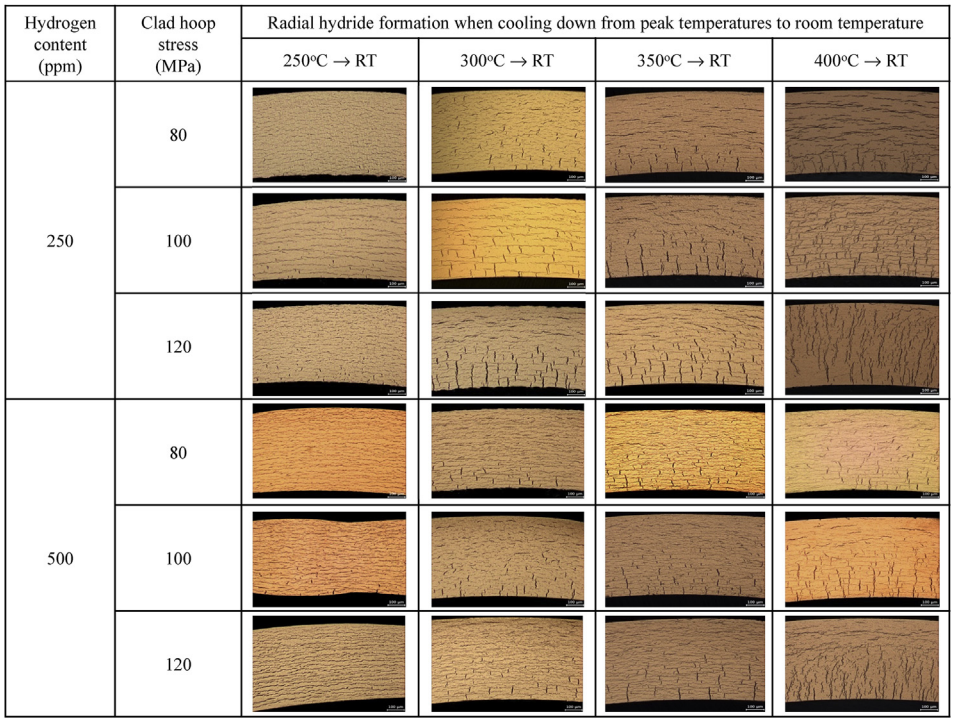

Fig. 6. Amount of radial hydride precipitation as a function of clad hoop stress during cool-down process from four peak cladding temperatures to room temperature for 250 ppm-H and 500 ppm-H specimens. RT, room temperature.

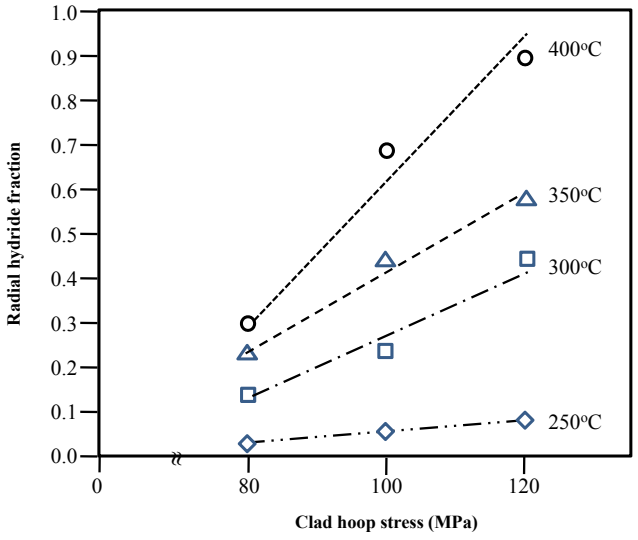

Fig. 7. Radial hydride fraction formed during cool-down process from four peak temperatures as a function of clad hoop stress for the 250 ppm-H specimens.

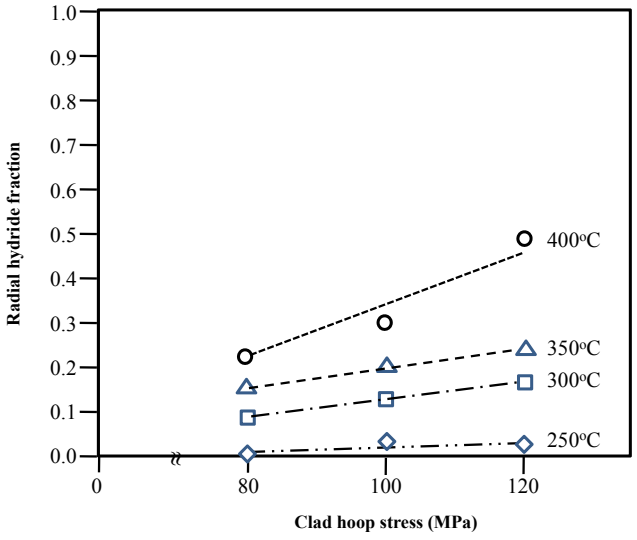

Fig. 8. Radial hydride fractions formed during the cool-down process from four peak temperatures as a function of clad hoop stress for the 500 ppm-H specimens.

specimens generated larger radial hydride fraction and longer radial hydride than did the 500 ppm-H specimens. In addition, the higher peak heat-up temperature and the higher tensile hoop stress generated a larger radial hydride fraction.

The amount of hydrides precipitated during the cool-down process depends on the TSSD (Terminal Solid Solubility for Dissolution) curve, although the TSSP (Terminal Solid Solubility for Precipitation) curve provides the temperature at which incipient precipitation will start during cool down (see the dotted curve in Fig. 4). As an example, when the specimens start to cool from 400°C to RT, the hydrogen atoms dissolved at 400°C do not form hydrides until ~340°C because the solubility line moves along line ①; then, the hydrogen solubility decreases along the dotted curve. Considering that the hydrogen solubilities at the peak temperatures of 250°C, 300°C, 350°C, and 400°C are 45 ppm, 80 ppm, 150 ppm, and 230 ppm, respectively, and that the hydrogen solubility at room temperature is ~10 ppm, the amount of hydrogen atoms precipitated during cool-down from the peak temperatures of 250°C, 300°C, 350°C, and 400°C to RT may be 35 ppm, 70 ppm, 140 ppm, and 220 ppm, respectively.

The phenomenon in which the 500 ppm-H specimens generated smaller radial hydride fractions than the 250 ppm-H

specimens may be explained by the relatively large amount of the undissolved circumferential hydrides in the 500 ppm-H specimens at the peak heat-up temperatures. The larger amounts of undissolved circumferential hydrides for the 500 ppm-H specimens may play an active role in blocking the growth of radial hydrides and subsequently limiting the radial hydride length to a level below the distance between adjoining circumferential hydrides. This may explain why the 500 ppm-H specimens generated a smaller fraction of radial hydrides precipitated during the cool-down and may also explain the shorter radial hydride length at the same cooling rate and tensile hoop stress.

The phenomenon in which a higher peak heat-up temperature generated a larger radial hydride fraction can be explained by the hydrogen solubility difference between the peak heat-up temperature and room temperature, as explained above.

The phenomenon in which a higher tensile hoop stress generated a larger radial hydride fraction can be explained as follows. The hydride orientation in the cladding tube is reported to be closely related to the cladding texture, manufacturing history, and cladding stress [9–11]. As shown in Table 1, the Kearns numbers of the Zr–Nb alloy cladding tubes are 0.62, 0.26, and 0.12 for the radial, tangential, and axial basal poles, respectively, indicating that the fraction of circumferential hydrides may be ~62%, in accordance with the Kearns number of 0.62 for a radial basal pole if there is no cladding stress effect on the hydride orientation. However, even when there is no cladding stress, hydrides are formed in the circumferential direction during the hydrogen charging process at 400°C, indicating that a certain threshold tensile hoop stress is needed for radial hydride formation during the cool-down process. Based on experimental results, it was reported that the threshold tensile hoop stress is between 75 MPa and 90 MPa for cladding temperatures between 250°C and 550°C [12,13]. The dissolved hydrogen atoms at the peak heat-up temperatures employed in this work precipitated during the cool-down process in the radial or circumferential directions; this process depended not only on the magnitudes of the radial or circumferential hydride nucleation energies but also on the nearest available sites of radial and circumferential hydride nucleation. As long as the applied hoop stress used in this work is larger than a certain threshold hoop stress, a higher tensile hoop stress may decrease the nucleation energy of the radial hydride precipitation but increase that of the circumferential hydride precipitation [14]. Therefore, a higher tensile hoop stress generated a larger radial hydride fraction during the cool-down process.

Figs. 9 and 10 show the hydrogen content-dependent plastic elongations for the 250 ppm-H and 500 ppm-H specimens. Using tensile hoop stress-strain curves, the plastic elongations were determined by subtracting the elastic strain from the total strain. As can be seen in these figures, the plastic elongation is ~28% at the peak temperature of 250°C and tensile hoop stress of 80 MPa; plastic elongation then decreases slightly with the increase of the tensile hoop stress to 120 MPa. However, the plastic elongation is nearly zero at the peak temperatures of 300°C, 350°C, and 400°C, regardless of the tensile hoop stress. These plastic elongation behaviors are related to radial hydride fractions, peak cladding temperatures, and tensile hoop stresses, as shown in Figs. 7 and 8. It was reported that for specimens having circumferential hydrides under tensile hoop stress state, the fracture is basically ductile [15,16]. This may be attributed to the fact that the shape of the hydrides is approximated as a flat oblate spheroid, and the transverse fracture of the circumferential hydrides produces a much smaller fractured area than that of the lengthwise fracture of the radial hydrides under tensile hoop stress state [17–19].

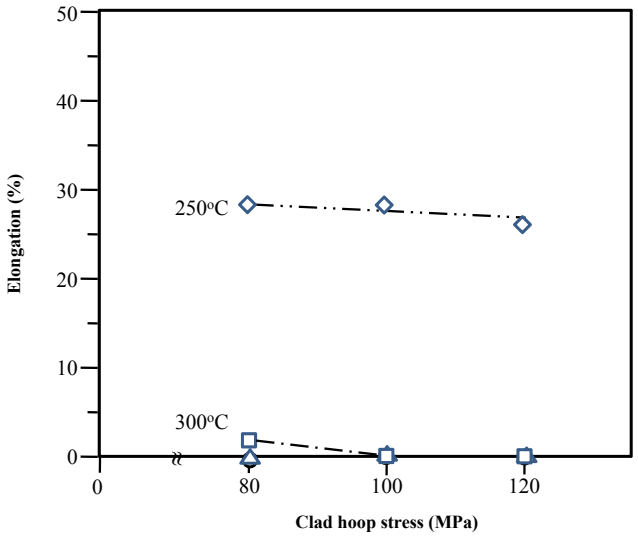

Fig. 9. Elongations of the cool-down specimens of 250 ppm-H having various radial hydride fractions as a function of clad hoop stress.

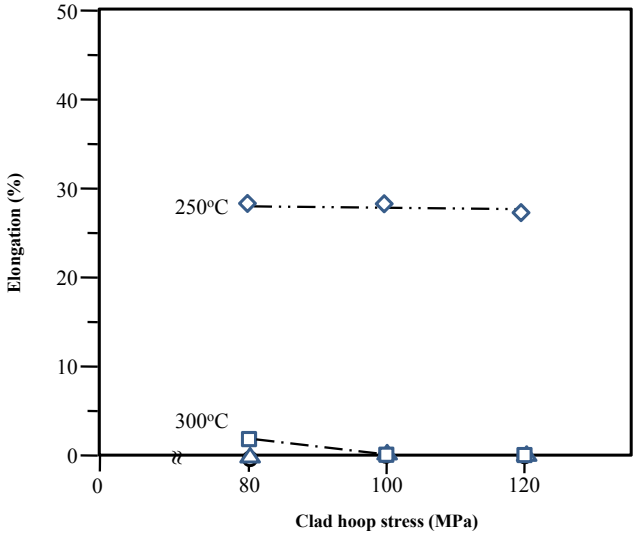

Fig. 10. Elongations of the cool-down specimens of 500 ppm-H having various radial hydride fractions as a function of clad hoop stress.

Therefore, radial hydrides are much more deleterious to zirconium-base alloy cladding tubes than are circumferential hydrides.

Based on the out-of-pile cladding tube test results mentioned above, it may be said that the peak cladding temperature occurring during interim-dry period should be limited to < 250°C; this temperature may be maintained via the use of a certain refrigerant during the vacuum dry process. However, it should be noted that the impact of irradiation, pellet-cladding bonding, and pellet stiffness on the allowable peak cladding temperature remains to be investigated to verify the peak cladding temperature of 250°C proposed in this study.

However, the fracture surfaces of the tensile-tested specimens were examined using a JEOL-6400 scanning electron microscope (SEM) provided by the McCRONE group at Westmont in Illinois in the U.S.A. The SEM micrographs of the fractured surfaces for the 250-ppm-H specimens are shown in Fig. 11. This

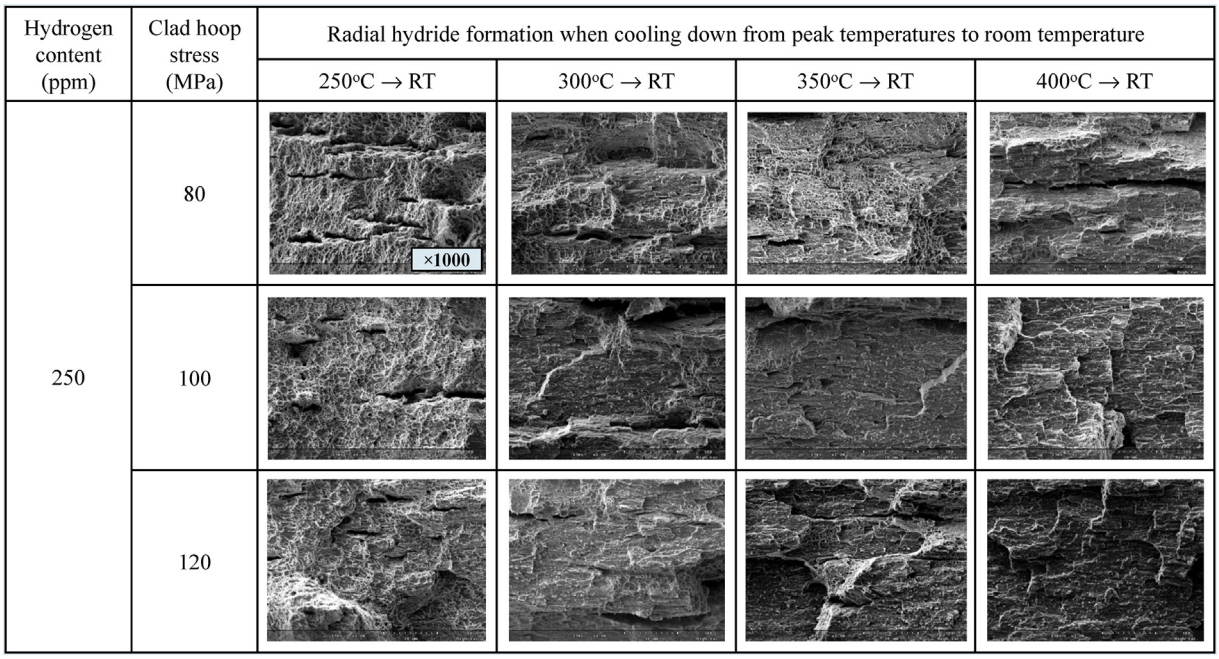

Fig. 11. SEM micrographs of fracture surfaces of the cool-down 250ppm-H specimens. RT, room temperature; SEM, scanning electron microscope.

figure indicates that specimens having lower peak temperature and tensile hoop stress generated more ductile fracture mode, which is characterized by dimple shapes, whereas those specimens having higher peak temperature and tensile hoop stress generated more brittle fracture mode, which is characterized by cleavage shapes.

4. Conclusion

The limiting factors for spent fuel cladding integrity maintenance during interim-dry storage and subsequent transport are investigated. The principal results obtained in this work can be summarized as follows: (1) the 500 ppm-H specimens generated smaller radial hydride fractions than the 250 ppm-H specimens when cooled from the four peak heat-up temperatures of 250°C, 300°C, 350°C, and 400°C to room temperature. This can be explained by the relatively larger amount of undissolved circumferential hydrides of the 500ppm-H specimens; (2) a higher peak heat-up temperature generated a larger radial hydride fraction when specimens were cooled to room temperature. This can be explained by the hydrogen solubility difference between peak heat-up temperature and room temperature. It should be noted that the hydrogen solubilities at the peak temperatures of 250°C, 300°C, 350°C, and 400°C are 45 ppm, 80 ppm, 150 ppm, and 230 ppm, respectively, and the hydrogen solubility at room temperature is ~10 ppm, so that the amount of hydrogen atoms precipitated during the cool-down process from the peak heat-up temperatures of 250°C, 300°C, 350°C, and 400°C to room temperature may be 35 ppm, 70 ppm, 140 ppm, 220 ppm, respectively; (3) a higher tensile hoop stress generated a larger radial hydride fraction when specimens were cooled from the four peak heat-up temperatures to RT. This may be because when the hoop stress applied to the cladding is larger than a certain threshold hoop stress, the higher tensile hoop stress may decrease the nucleation energy for radial hydride precipitation, but may increase the nucleation energy for circumferential hydride precipitation; the plastic elongations of the cool-down specimens are nearly zero when specimens were cooled from the peak heat-up temperatures of 300°C, 350°C, and 400°C, regardless of the tensile hoop stress. These behaviors are directly related to the radial hydride fractions and are functions of the peak heat-up cladding temperature. Based only on these cladding tube out-of-pile test results, it may be said that the peak cladding temperature during interim-dry storage should be limited to a level < 250°C, even though more detailed experiments to determine such aspects as impact of irradiation, impact of pellet-cladding bond, and impact of pellet stiffness when contact between pellet and cladding occurs, remain as subjects of future research that will need to be conducted to verify the proposed peak cladding temperature.

Conflicts of interest

The authors have no conflicts of interest to declare.

Acknowledgments

This work was supported by the Dongguk University Research Fund of 2016 (K-2016-000895). This work was also supported by Nuclear Energy Development Program (Nos. 2016M2A8A4021567 and 2016M2A8A6900464) through the National Research Foundation of Korea (NRF) funded by the Ministry of Science, ICT, and Future Planning.

References

[1] H. Cha, K. Jang, J. An, K. Kim, The effect of hydrogen and oxygen contents on hydride reorientations of zirconium alloy cladding tubes, Nucl. Eng. Technol. 47 (2015) 746–755.
[2] S. Min, J. Won, K. Kim, Terminal cool-down temperature-dependent hydride reorientations in Zr–Nb Alloy claddings under dry storage conditions, J. Nucl. Mater. 448 (2014) 172–183.
[3] T.L. Sanders, K.D. Seager, Y.R. Rashid, P.R. Barrett, A.P. Malinauskas, R.E. Einziger, H. Jordan, T.A. Duffey, S.H. Sutherland, P.C. Reardon, A Method of Determining the Spent-fuel Contribution to Transport Cask Containment Requirements, SAND90–2406, November 1992.
[4] J. Won, M. Kim, K. Kim, Heat-up and cool-down temperature-dependent hydride reorientation behaviors in zirconium alloy cladding tubes, Nucl. Eng. Technol. 46 (2014) 681–688.
[5] USNRC [Internet]. Interim Staff Guidance, Cladding Considerations for Transportation and Storage of Spent Nuclear Fuel, ISG-11, Revision 3, November

2003. Available from: https://www.nrc.gov/reading-rm/doc-collections/isg/isg-11R3.pdf.
[6] H. Kim, Y. Jeong, K. Kim, The effects of creep and hydride on spent fuel integrity during interim-dry storage, Nucl. Eng. Tchnol. 42 (2010) 249–258.
[7] H. Kim, I. Kim, S. Park, J. Park, Y. Jeong, Evaluation of hydride effect on fuel cladding degradation, Kor. J. Met. Mater. 48 (2010) 717–724.
[8] P. Vizcaíno, P. Bozzano, A. Flores, A. Banchik, R. Versaci, R. Ríos, Hydrogen solubility and microstructural changes in Zircaloy-4 due to neutron irradiation, J. ASTM Int. 8 (2011) 1–20.
[9] R. Marshall, M. Louthan Jr., Tensile properties of Zircaloy with oriented hydrides, Trans. ASM 56 (1963) 693–700.
[10] R. Marshall, Control of hydride orientation in Zircaloy by fabrication practice, J. Nucl. Mater. 24 (1967) 49–59.
[11] J. Kearns, C. Woods, Effect of texture, grain size, and cold work on the precipitation of oriented hydrides in Zircaloy tubing and plate, J. Nucl. Mater. 20 (1966) 241–261.
[12] K. Colas, A. Motta, J. Almer, M. Daymond, M. Kerr, A. Banchik, *In situ* study of hydride precipitation kinetics and reorientation in Zircaloy using synchrotron radiation, Acta Mater. 58 (2010) 6575–6583.
[13] H. Chung, Fundamental metallurgical aspects of axial splitting in Zircaloy cladding, in: Proc. Int. Topical Meeting on Light Water Reactor Fuel Performance, 2000, p. 325. Park City, Utah, USA.
[14] W. Qin, J. Szpunar, J. Kozinski, Hydride-induced degradation of hoop ductility in textured zirconium-alloy tubes: a theoretical analysis, Acta Mater. 60 (2012) 4845–4855.
[15] R. Bourcier, D. Koss, Hydrogen embrittlement of titanium sheet under multi-axial states of stress, Acta Metall. 32 (1984) 2091–2099.
[16] Y. Fan, D. Koss, The influence of multi-axial states of stress on the hydrogen embrittlement of Zr alloy sheet, Metall. Trans. A 16 (1985) 675–681.
[17] D. Northwood, U. Kosasih, Hydrides and delayed hydrogen cracking in zirconium and its alloys, Int. Met. Rev. 28 (1983) 92–121.
[18] G. Itoh, M. Kanno, T. Hagiwara, T. Sakamoto, Embrittlement in an age-hardened 2091 aluminum alloy by exposure at elevated temperatures below the aging temperature, Acta Mater. 47 (1999) 3799–3809.
[19] V. Perovic, G. Weatherly, C. Simpson, Hydride precipitation in α/β zirconium alloys, Acta Metall. 31 (1983) 1381–1391.